

Pressure-induced loss of electronic interlayer state and metallization in ionic solid Li_3N

A. Lazicki,^{1,2,*} C. W. Yoo,^{1,†} W. J. Evans,¹ M. Y. Hu,³ P. Chow,³ and W. E. Pickett²

¹*Lawrence Livermore National Laboratory, Livermore, California 94550*

²*Physics Department, University of California, Davis, California 95616*

³*HPCAT/APS, Argonne National Laboratory, Argonne, Illinois 60439*

X-ray diffraction and nitrogen K-edge X-Ray Raman Scattering (XRS) investigations of the crystal and electronic structure of ionic compound Li_3N across two high pressure phase transitions are conducted in a diamond anvil cell and results interpreted using density functional theory. A low-energy peak in the XRS spectrum which is observed in both low-pressure hexagonal phases of Li_3N and absent in the high pressure cubic phase is found to originate from an interlayer band similar to the important free-electron-like state present in the graphite and graphite intercalated systems, but not observed previously in ionic insulators. XRS detection of the interlayer state is made possible because of its strong hybridization with the nitrogen p-bands. A pressure-induced increase in the band gap of the high pressure cubic phase of Li_3N is explained by the differing pressure dependencies of different quantum-number bands and is shown to be a common feature in similar low-Z closed-shell ionic materials.

I. INTRODUCTION

Lithium nitride is the only known thermodynamically stable alkali metal nitride and is one of the most ionic of all known nitrides. At ambient pressure, the nitrogen exists in the multiply charged (N^{3-}) state [1, 2] considered to be stable only because of its crystal environment - a hexagonal bipyramid of Li^+ ions [3, 4] unique to the N ion. This material is a superionic conductor via vacancy-induced Li^+ diffusion within the Li_2N layers [5–7]. Its potential for use as an electrolyte in lithium batteries [4], a hydrogen storage medium [8–11] and a component in the synthesis of GaN [12] have prompted several studies including investigations into its behavior at high pressure [13, 14].

It has been demonstrated that Li_3N retains its ionic character up to very high pressure, while undergoing a significant structural transition [14]. Inelastic X-ray scattering experiments as well as first-principles calculations reveal that this structural change is accompanied by distinct changes in the electronic bands. Electronic changes accompanying pressure-driven structural phase transitions in covalently bonded materials (such as graphite and boron nitride) are relatively well understood because their directional bonding is affected in a predictable way by changes in the local crystal environment. However, in non-directionally-bonded closed-shell ionic materials the situation is more subtle and electronic changes not as well documented. Here we explore the origins of these changes and identify an important feature in the band structure; an interlayer band (to our knowledge, reported here for the first time in an ionic solid) which was previously understood to have Li 2s character [1].

A pressure-driven widening of the electronic band gap is examined and related to an expected rapid increase in energy of the conduction bands relative to the valence bands as a result of their lack of d-character, higher principle quantum number and kinetic energy. Neighboring ionic insulators Li_2O and LiF are shown to demonstrate similar behavior under pressure.

II. TECHNIQUES

Angle-dispersive X-ray diffraction and nitrogen K-edge X-ray Raman spectroscopy experiments were conducted in the diamond anvil cell up to 200 GPa. Experimental details have been reported in [14].

First-principles electronic structure calculations were performed to explore and clarify the electronic changes occurring under pressure. Because of the large six-fold compression carried out in these calculations, we used two methods for comparison: full-potential linearized augmented plane-waves (LAPW) as implemented in WIEN2k code [18] within the Generalized Gradient Approximation [20] and a full-potential nonorthogonal local-orbital minimum basis band structure scheme (FPLO) [19], within the local spin-density approximation (LSDA) [21]. For the LAPW calculation, muffin tin radii (R_{mt}) were set so that neighboring muffin tin spheres were nearly touching at each volume, and the plane wave cutoff K_{max} was determined by $R_{mt}K_{max} = 9.0$. The Brillouin zone was sampled on a uniform mesh with 185 irreducible k-points. The energy convergence criterion was set to 0.1 mRy. For both calculations we found it necessary to put the lithium 1s core electrons into the valence states. Thus, in the FPLO scheme, Li 1s, 2s, 3p, 3s, 3p and 3d states and N 2s, 2p, 3s, 3p and 3d states were used as valence states and only the lower-lying N 1s state was treated as a core state. The results of these two codes are in good agreement.

*Now at: Geophysical Laboratory, Carnegie Institution of Washington, Washington DC 20015

†Now at: Washington State University, Pullman, Washington 99164

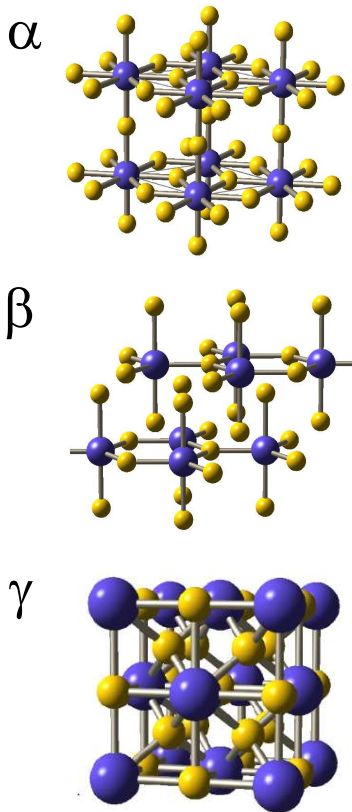


FIG. 1: (Color online) Crystal structures of each phase with larger spheres representing the nitrogen ions, smaller representing lithium.

III. RESULTS

A. X-ray Diffraction

X-ray diffraction results identified the structures shown in Figure 1. At ambient conditions, the powder sample exists as a combination of two hexagonal phases known as α - Li_3N (P6/mmm) and metastable β - Li_3N (P6₃/mmc). α - Li_3N fully transforms to β - Li_3N near 0.5 GPa, and a second phase transition to a cubic phase, γ - Li_3N (Fm3m), occurs near 40 GPa. The cubic phase can be understood as the rocksalt structure with the two additional Li ions occupying the tetrahedral holes in the lattice.

In Figure 2, experimental data showing the change in volume as a function of pressure for β - and γ - Li_3N are fit with the 3rd order Birch-Murnaghan equation of state. Fitting parameters (summarized in [14]) agree well with results from the DFT calculated equation of state, which is shown as the dotted curve in Figure 2. The good agreement between experiment and theory indicates that the approximations made in the calculations are appropri-

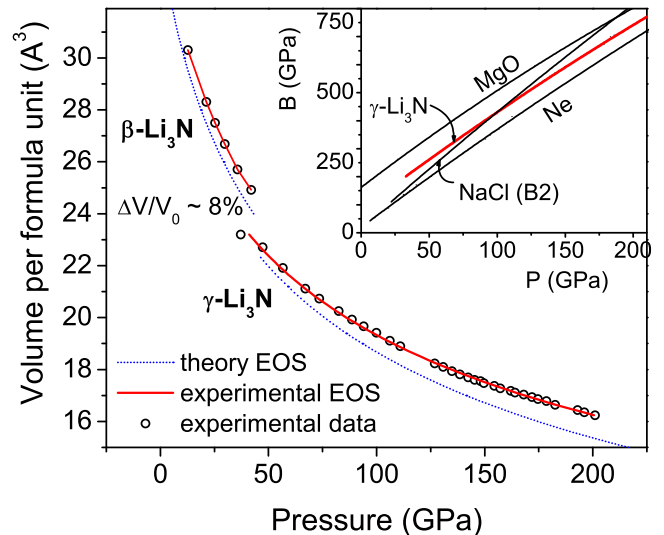


FIG. 2: (Color online) Experimental and calculated equation of state of β - and γ - Li_3N . In the inset, the high pressure bulk modulus of γ - Li_3N is compared to other common highly compressible materials. [22, 23] (NaCl, MgO and Ne Curves are interpolated up to 200 GPa).

ate for this system. Moderate differences between experimental and calculated equation of state in the cubic phase may be attributed to the lack of a hydrostatic pressure medium, or to some overbinding by the GGA exchange-correlation functional. Negligible broadening of the diffraction peaks between 43 and 200 GPa in the γ phase was observed, indicating little inhomogeneous strain and, therefore, quasi-hydrostatic conditions.

In the inset of Figure 2 we examine the change in bulk modulus (the inverse of the compressibility) as a function of pressure for cubic Li_3N and compare it with isoelectronic neon, as well as other well-known and highly compressible closed-shell ionic solids. The cubic phase follows the same trend in compressibility as inert neon, indicating that the coulomb interactions are well balanced in this isotropic crystal structure, and the closed-shell ionic state is stabilized to surprisingly high pressure. For further details concerning the structural phase transitions, see [14].

B. X-ray Raman Scattering

While structurally similar to the graphite-diamond and hexagonal-cubic BN transitions, the different bonding in Li_3N (ionic rather than covalent) led us to examine the electronic structure with X-ray Raman spectroscopy (XRS), with which one can probe the K-shells of low-Z materials (in our case, nitrogen). The acquired spectra (Figure 3) describe the density of electronic transitions from the nitrogen core to the lowest lying unoccupied

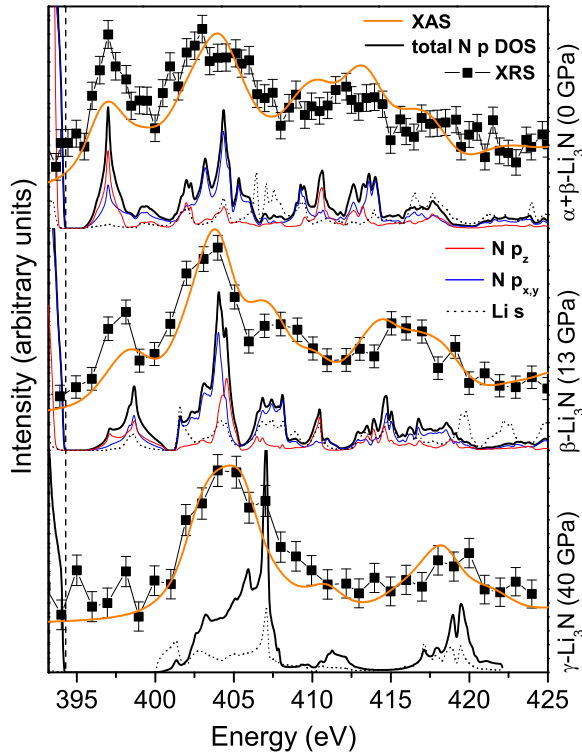


FIG. 3: (Color online) Measured nitrogen k-edge XRS spectra from the three phases of Li_3N compared with calculated Nitrogen p and Lithium s projected density of states and with the calculated X-ray absorption spectrum. The calculated curves were offset by 394.2 eV (arbitrary) in every case, for the sake of qualitative comparison with the experimental results. The vertical dashed line indicates the calculated energy of highest occupied valence states.

conduction states. In the case of the covalently bonded materials, the XRS spectrum is characterized by two distinct features: a sharper peak at lower energy which has been shown to correspond to transitions to π^* molecular orbital states, and a broader peak at higher energy which describes transitions to σ^* states [26–28]. The phase transition from a layered hexagonal structure such as sp^2 -bonded graphite to a sp^3 -bonded cubic structure such as diamond is accompanied by loss of the π^* bonding states. Therefore, one sees the narrower lower energy peak disappear across the hexagonal-cubic transition in the covalently bonded compounds. The data acquired for Li_3N (Figure 3) show the same characteristic leading edge peak in both hexagonal phases and not in the cubic phase.

However, the calculated spectra reveal some important differences. Within the dipole approximation the nitrogen K-edge XRS should give us a reasonably good approximation of the X-ray absorption spectrum. We therefore calculated this quantity from the nitrogen p projected density of states multiplied by the dipole-allowed

transition matrix elements and a transition probability (Figure 3). The important features in the experimental spectrum are reproduced in the calculated X-ray absorption spectrum and in the nitrogen p projected density of states. The projected density of states is shown for the purpose of demonstrating that the leading edge peak (which, in the case of graphite, represents a π^* bonding state of almost entirely C p_z character [29]) is composed of similar contributions from p_z and p_x+p_y . This indicates that the nitrogen p states in hexagonal Li_3N are energetically less distinguishable; their distribution is close to spherically symmetric, with little directional character. This evidence supports a closed-shell ionic state and raises questions about the nature of this leading edge peak. Why is it present in the hexagonal phase and not in the cubic, if the p electron states are not significantly affected by the local coordination?

Electronic structure interpretations of ambient Li_3N from previous work claim that the electronic bands from which this density arises have Li 2s character [1]. We plot the band structures for the three phases (Figure 4). In the α phase, the band has a minimum with parabolic character around the Γ point and Γ_1^+ (s-like) symmetry. β - Li_3N has two formula units per primitive cell, so the (symmetric) Γ_1^+ band folds back at the Brillouin zone boundary, giving rise to a second band with (antisymmetric) Γ_3^+ symmetry (notation taken from Robertson [30]). The projected density of states in Figure 3 shows a small Li s-character that does not support a “Li 2s” characterization of this state. Moreover, the density plots in Figs. 5 and 6 clearly show there is no 2s-like density around the Li ions that is distinct from the main density in the interstitial region.

IV. DISCUSSION

We interpret the character of the lowest conduction band in the hexagonal phases (Figure 4) by comparison with analogous bands in graphite, graphite intercalates and hexagonal boron nitride. These latter materials, in addition to the π^* and σ^* states in the absorption spectrum, possess a smaller and weaker peak, the existence of which has been long known but generally ignored because of its overlap with the much more dominant sp bands [31–33]. Its character, however, is well understood and in fact very recently it has been suggested to play a vital role in the superconductivity of the lithium intercalated graphite compounds [34]. This band (of Γ_1^+ symmetry) is a free-electron-like interlayer (IL) state, given that its probability density peaks in interstitial regions between the hexagonal layers and cannot be assigned to a particular atomic character. The density in these compounds is more strongly mixed into other electronic bands than is the case in Li_3N , where it is excluded from the region of N^{3-} charge both by electron repulsion and by kinetic energy effects (basically orthogonalization). However this state still manages to hybridize with the tails of the N 2p

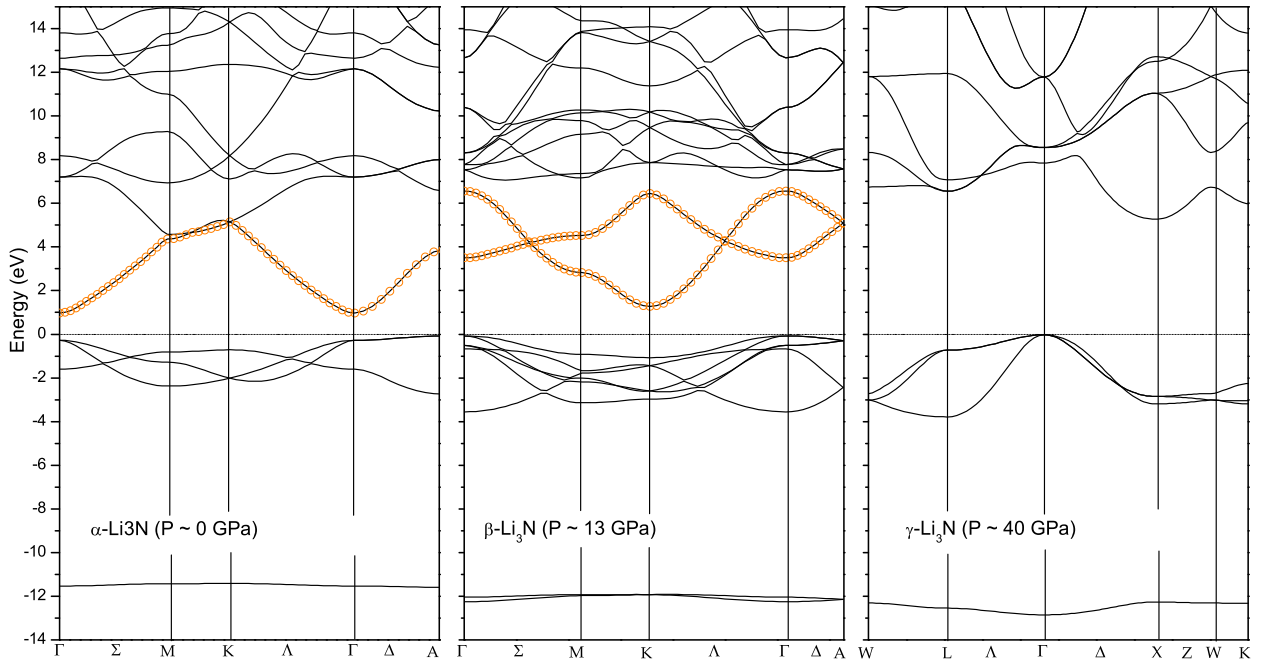


FIG. 4: (Color online) Calculated electronic band structure for the three phases of Li_3N , with the interlayer band highlighted in orange in the two hexagonal phases.

orbitals.

Examination of the density originating from the IL band in Li_3N (Figures 5 and 6) indeed verifies, in the hexagonal phases, a concentration in the more open interstitial regions between the hexagonal planes. However, the IL bands in this material differ from those seen in graphite and graphite intercalates and also h-BN. The effective band masses at the conduction band minima for α and β - Li_3N are $0.36m_0$ and $0.46m_0$, respectively, which is significantly lighter than for strictly free electron-like behavior. Also, the IL bands show a dispersion along k_z (Γ -A) comparable to the in-plane dispersion, indicating that the states are connected through the interstitial holes in the hexagonal layers of N ions in this material. Between 0 and 35 GPa in the β phase, the energy of the IL band (particularly at the minimum at K) changes little (Figure 7) while the lithium intercalates' IL state is sensitive to the c-axis lattice constant [34, 35]. The insensitivity to pressure (i.e. interstitial volume) and the light mass of the IL bands of hexagonal Li_3N phases may be due to the presence of Li ions between the layers, which do provide a non-constant (albeit weak) pseudopotential and do exclude the IL density from the $1s$ core region.

Within the dipole approximation (limit of small momentum transfer q), the N k -edge XRS spectrum should show only final states with N $2p$ character. In our case ($q \sim 2.2 \text{ \AA}^{-1}$) this approximation is reasonably good. Transitions to the IL state are allowed because there are linear combinations of the IL states at various k points that

will have the same symmetry as the N $2p$ states, and thus will hybridize with it. The intensity of the leading edge peak is a measure of the degree of that hybridization. The XRS spectrum, therefore, provides an indirect, semiquantitative measure of the presence of an IL state.

The IL band interpretation could explain the lack of sharp onset to the leading edge peak often seen in XRS due to excitonic effects. In cases where the electronic transition is $1s \rightarrow \pi^*$ on a single atom, the core hole and electron are in close enough proximity for an exciton to be created. In a transition to the more distant IL region, however, such effects are less likely [36].

Based on our interpretation of the IL state and its existence due to layered interstitial regions containing only Li ions, the large increase in band gap across the phase transition from hexagonal β - Li_3N to cubic γ - Li_3N can be understood simply as a loss of the IL band in the more close-packed cubic phase; the other conduction bands still lie at the same energy.

The large bandgap increase is evident experimentally from the change in optical absorption near the phase transition (Figure 8), which was also observed by Ho et al. [13]. The calculated band gap increases from $\beta \rightarrow \gamma$ is 1.5 to 5.5 eV (the GGA underestimate of the gap is well known). At 5.5 eV one may expect to see a completely transparent sample but, in fact, we see a strong yellow-orange tint. Factors such as absorption from a color center produced by Li vacancies (which are indeed predicted in the hexagonal phases, as a driving force for superionic

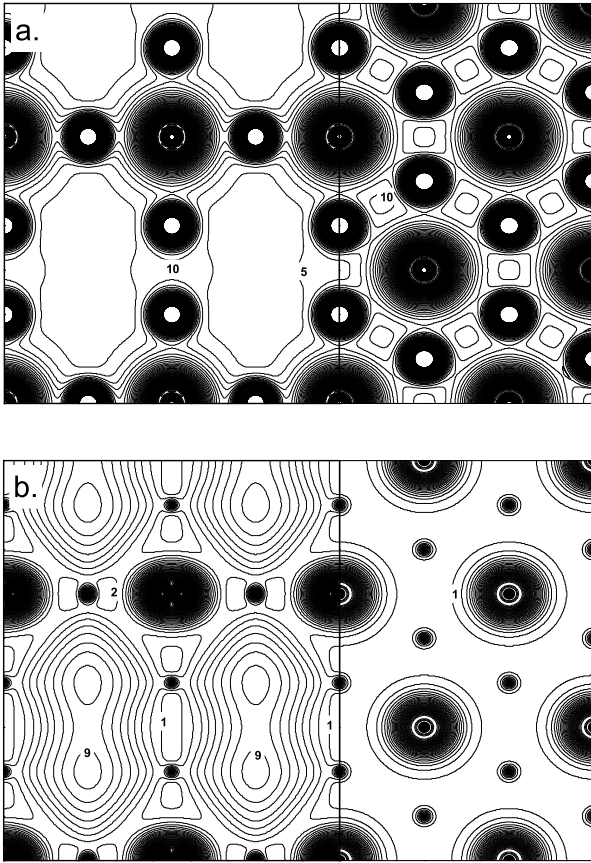


FIG. 5: α - Li_3N valence density (a) and (unoccupied) inter-layer band density (b) contours perpendicular to the basal plane (left panels) and within the basal plane (right panels). Large regions of white space in (a) signify very low density whereas the contours in the same areas in (b) denote a maximum in the IL density. Contours are labeled in units of $0.01 e/\text{\AA}^3$ and separated by $0.05 e/\text{\AA}^3$ (a) and $0.01 e/\text{\AA}^3$ (b).

conductivity [37]) could cause such a coloration.

The calculated behavior of the γ - Li_3N band gap upon further increase of pressure is shown in Figure 9. As volume is reduced, the 5.4 eV indirect fundamental gap between Γ and X begins to increase rapidly, passing the band minimum at L near $V/V_0 = 0.4$. The Γ - L indirect gap continues to increase more slowly up to 8.2 eV at $V/V_0 = 0.22$ (calculated pressure of ~ 760 GPa), before finally beginning to collapse. Metallization via closing of the Γ - L gap finally occurs at $V/V_0 = 0.08$ (calculated pressure near 8 TPa, which is a lower limit due to the GGA underestimation of band gaps.) The gap closing is due to broadening of the valence and conduction bands; the band centers continue to separate throughout the entire range of pressure. At the onset of metallization the N 2p upper valence states have broadened by a factor of 8.

To give some perspective on how high the metallization pressure is for γ - Li_3N , some of the highest metallization

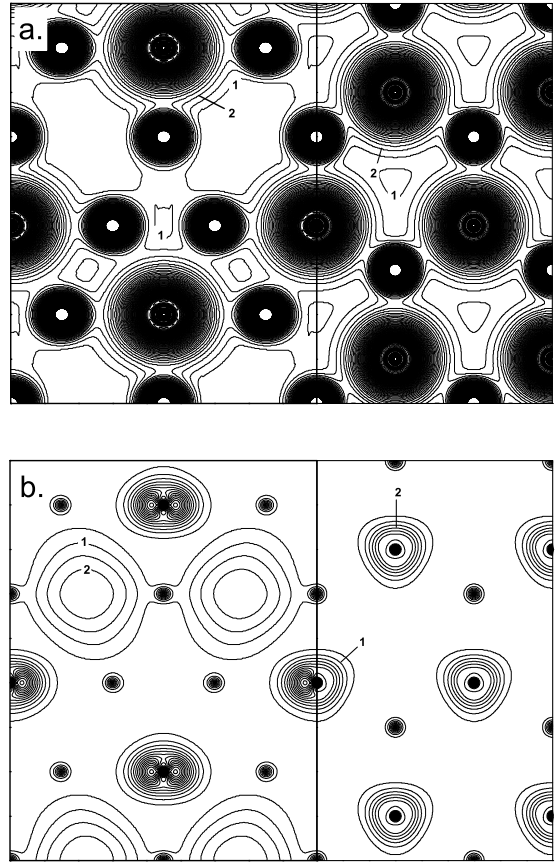


FIG. 6: β - Li_3N valence density (a) and (unoccupied) inter-layer band density (b) contours perpendicular to the basal plane (left panels) and within the basal plane (right panels). Large regions of white space in (a) signify very low density whereas the contours in the same areas in (b) denote a maximum in the IL density. Contour lines are labeled in units of $0.1 e/\text{\AA}^3$ and separated by $0.05 e/\text{\AA}^3$.

pressures that have ever been predicted are for other cubic close-shelled solids Ne, MgO and NaCl at 134 TPa, 21 TPa and 0.5 TPa, respectively [41–43]. Clearly, γ - Li_3N fits well into this family. This analysis neglects the possibility of an additional structural phase transition for Li_3N at higher pressures. An fcc to orthorhombic transition is conceivable [25]; however, from the example of He [44], this may not significantly effect the metallization pressure.

A band gap increase under pressure is observed in many other semiconducting materials; particularly the tetrahedrally coordinated zincblende and wurtzite structures such as diamond [45], group III nitrides [46, 48], and others [47]. Several effects contribute to the gap increase in these cubic semiconductors. Of primary importance is the presence of d-like states in the lower conduction or upper valence bands. The mechanism for metallization in most higher-Z ionic, insulating compounds is the strong relative decrease in energy of the conduction d bands rel-

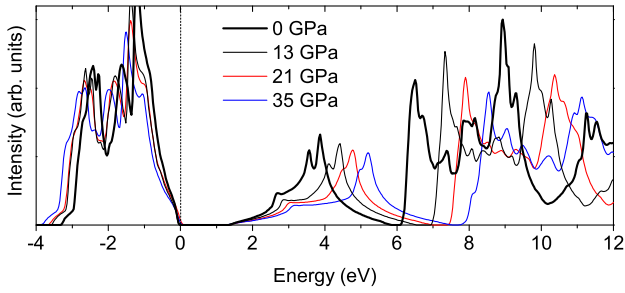


FIG. 7: (Color online) Total density of states of valence and low-lying conduction bands of β - Li_3N between 0 and 35 GPa.

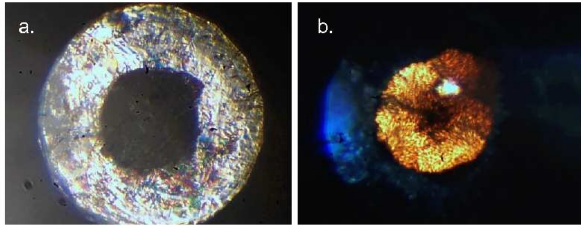


FIG. 8: (Color online) Sample image at ambient pressure (a) and at the $\beta \rightarrow \gamma$ phase transition near 40 GPa (b). The bright spot at 40 GPa is the ruby grain used for pressure calibration.

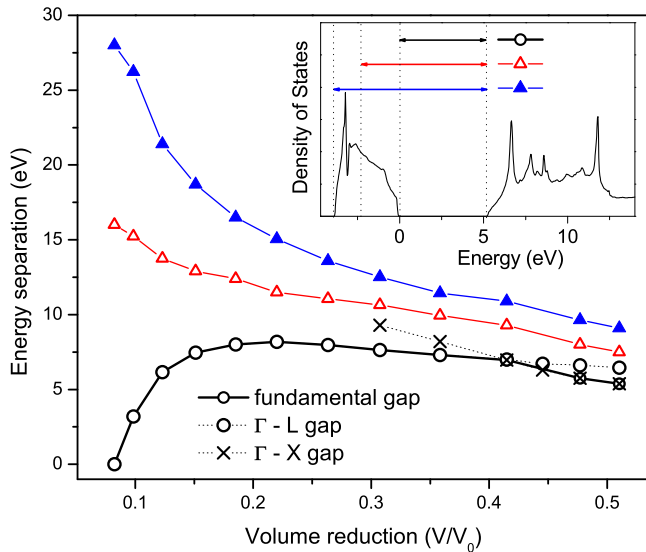


FIG. 9: (Color online) Change in valence band energies relative to bottom of the conduction band in the γ phase from the phase transition to metallization. Energy gaps explained in the density of states plot (inset): open circles give the fundamental band gap, and the energy separation between the bottom of the conduction band and the center of mass of the valence band (open triangles) and the bottom of the valence band (closed triangles) are also shown. V_0 is the volume of α - Li_3N at ambient pressure.

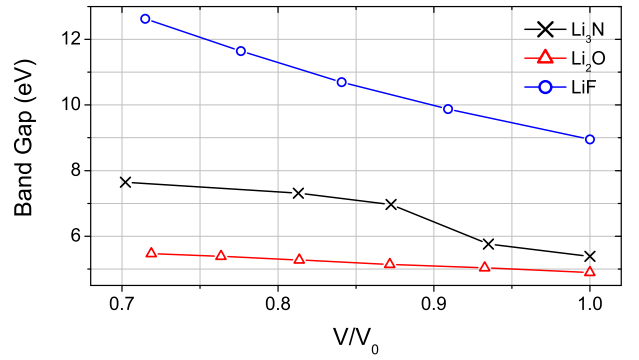


FIG. 10: Band gap increases as a function of volume reduction for related close-shelled cubic Li compounds. LiF and Li_2O are cubic at ambient pressure and V_0 refers to the ambient pressure volume. Li_3N V_0 (in this instance alone) is taken as the volume at the $\beta \rightarrow \gamma$ phase transition.

ative to the s and p valence bands, leading to eventual transfer of electrons from d to s across the Fermi level, or hybridization between these states [49]. The reason for the record-breaking metallization pressure predicted for Ne is that the band overlap does not occur until the $3s$ and $3p$ conduction bands, to finally overlap the $2p$ valence bands at an astonishing 34-fold volume compression. This is an example of a more general trend; that bands with higher total energy (related to principle quantum number n) will increase in energy with respect to lower bands, and that bands with smaller ℓ (orbital character) increase in energy with respect to larger ℓ [49]. Indirect-gap cubic Li_3N (as well as neighboring cubic Li compounds for which we also calculated a gap increase under pressure in Figure 10, consistent with the findings of [52, 53]) have completely filled $1s$ shells on the lithium ions and $2p$ shells on the anion. The low-lying conduction bands, therefore, consist of entirely Li $2s/2p$ character and anion $3s/3p$ character (and negligibly small d character anywhere near the band gap), which can be expected to increase in energy more rapidly than the lower-quantum number valence states, resulting in the observed band gap increase in all three of these cubic compounds.

Larger band broadening in γ - Li_3N compared to Ne due to the presence of Li ions within the fcc N^{3-} lattice results in gap closure for Li_3N at much lower compression than for Ne, long before d bands begin to overlap the valence states. This, as well as the existence of Li character in the conduction bands which makes the phenomenon more of an interspecies metallization in Li_3N , contribute to the lower metallization pressure than predicted for Ne.

The apparent correlation between cubic structure and increasing band gap can be explained in a few ways. For rocksalt compounds that do possess low-lying d bands, inversion symmetry forbids the p - d interaction at the Γ point, resulting in a repulsion between these bands at $k=0$. Subsequently, the direct gap increases as a function

of pressure, but indirect gaps decrease as the d bands are allowed to hybridize [50, 51]. However, for the case of gap increase in the cubic phase of Li_3N (whereas the hexagonal phases show an unchanged or decreasing gap) the argument for relative trends in bands of differing orbital character appears to hold in all phases, and the fact that the fundamental gap in the hexagonal phases does not increase seems to be due simply to the more rapid band broadening. The gap between the conduction and valence states is in fact increasing in the hexagonal phases, as seen in Figure 7, but the rapid broadening of the interlayer bands as a result of the decrease in interlayer spacing (decreasing c/a ratio) causes an overall decrease in the fundamental gap.

V. CONCLUSION

Ionic solid Li_3N is demonstrated to possess large concentrations of unoccupied charge states in the open interlayer regions of the hexagonal phases, which result in low-lying conduction bands of the variety previously observed in layered covalently bonded compounds but not to our knowledge previously seen in ionic materials. The

strong hybridization between the interlayer state and nitrogen p states allows its detection with X-ray Raman spectroscopy. The large band gap increase across the hexagonal-cubic phase transition is then interpreted as a loss of the interlayer band. Further increase of the band gap as pressure is increased is related to the rapid upward shift of the lower conduction bands relative to the valence bands, by reason of their higher angular momentum character.

VI. ACKNOWLEDGMENTS

We acknowledge A. K. McMahan, B. J. Baer, J. Seidler and A. Libál for advice and useful discussions during this investigation. Use of the HPCAT facility was supported by DOE-BES, DOE-NNSA (CDAC), NSF, DOD-TACOM, and the W. M. Keck Foundation. We thank HPCAT beamline scientist M. Somayazulu for technical assistance. This work has been supported by the LDRD(04ERD020) and SEGRF programs at the LLNL, University of California under DOE No. W7405-ENG-48 and by the SSAAP (DE-FG03-03NA00071) and NSF(ITR 031339) at UCD.

-
- [1] G. Kerker, Phys. Rev. B **23**, 6312 (1981)
- [2] R. Dovesi, C. Pisani, F. Ricca, C. Roetti and V. R. Saunders, Phys. Rev. B **30**, 972 (1984).
- [3] E. Zintl and G. Brauer, Z. Elektrochem, **41**, 102 (1935).
- [4] A. Rabenau and H. Schulz, J. Less Common Metals **50**, 155 (1976); A. Rabenau, Solid State Ionics **6**, 277 (1982).
- [5] M. L. Wolf, J. Phys. C: Solid State Phys. **17**, L285 (1984).
- [6] J. Sarnthein, K. Schwarz and P. E. Blöchl, Phys. Rev. B **53**, 9084 (1996).
- [7] E. Bechtold-Schweickert, M. Mali, J. Roos and D. Brinkmann, Phys. Rev. B **30**, 2891 (1984).
- [8] P. Chen, Z. Xiong, J. Luo, J. Lin and K. L. Tan, Nature **420**, 302 (2002).
- [9] T. Ichikawa, S. Isobe, N. Hanada and H. J. Fujii, J. Alloys Compd. **365**, 271 (2004).
- [10] Y. H. Hu and E. Ruckenstein, Ind. Eng. Chem. Res. **44**, 1510 (2005).
- [11] Y. Nakamori, G. Kitahara, K. Miwa, S. Towata and S. Orimo, Appl. Phys. A: Mat. Sci. Process. **80**(1): 1 (2005).
- [12] Y. Xie, Y. T. Qian, W. Z. Wang, S. Y. Zhang and Y. H. Zhang, Science **272**, 1926 (1996).
- [13] A. C. Ho, M. K. Granger, A. L. Ruoff, P. E. Van Camp and V. E. Van Doren, Phys. Rev. B **59**, 6083 (1999).
- [14] A. Lazicki, B. Maddox, W. J. Evans, C.-S. Yoo, A. K. McMahan, W. E. Pickett, R. T. Scalettar, M. Y. Hu and P. Chow, Phys. Rev. Lett. **95**, 165503 (2005).
- [15] A. P. Hammersley, ESRF Internal Report, ESRF97HA02T, "FIT2D: An Introduction and Overview", (1997).
- [16] S. Desgreniers and K. Lagarec, J. Appl. Cryst. **27**, 432 (1994).
- [17] B. H. Toby, J. Appl. Cryst. **34**, 210 (2001).
- [18] P. Blaha et al., *WIEN2k*, Karlheinz Schwarz, Techn. Universität Wien, Wien (2001).
- [19] K. Koepf and H. Eschrig, Phys. Rev. B **59**, 1743 (1999).
- [20] J. P. Perdew, K. Burke, and M. Ernzerhof, Phys. Rev. Lett. **77**, 3865 (1996).
- [21] J. P. Perdew and Y. Wang, Phys. Rev. B **45**, 13244 (1992).
- [22] N. Sata, G. Shen, M. L. Rivers and S. R. Sutton, Phys. Rev. B **65**, 104114 (2002).
- [23] R. J. Hemley et al., Phys. Rev. B **39**, 11820 (1989).
- [24] H. J. Beister, S. Haag, R. Kniep, K. Strossner and K. Syassen, Angew. Chem. Int. Ed. **27**, 1101 (1988).
- [25] J. C. Schön et al., J. Mater. Chem. **11**, 69 (2001).
- [26] Y. Meng, H. Mao, P. J. Eng, T. P. Trainor, M. Newville, M. Y. Hu, C. Kao, J. Shu, D. Hausermann and R. J. Hemley, Nat. Mater. **3**, 111 (2004).
- [27] S. K. Lee, P. J. Eng, H. Mao, Y. Meng, M. Newville, M. Y. Hu and J. Shu, Nat. Mater. **4**, 851 (2005).
- [28] U. Bergmann, O. C. Mullins and S. P. Cramer, Anal. Chem. **72**, 2609 (2000).
- [29] P. E. Batson, Phys. Rev. B **48**, 2608 (1993).
- [30] J. Robertson, Phys. Rev. B **29**, 2131 (1984).
- [31] A. Catellani, M. Posternak, A. Baldereschi, H. J. F. Jansen and A. J. Freeman, Phys. Rev. B **32**, 6997 (1985).
- [32] B. Reihl, J. K. Gimzewski, J. M. Nicholls and E. Tosatti, Phys. Rev. B **33**, 5770 (1986).
- [33] Th. Fauster, F. J. Himpsel, J. E. Fischer and E. W. Plummer, Phys. Rev. Lett. **51**, 430 (1983).
- [34] G. Csányi, P. B. Littlewood, A. H. Nevidomskyy, C. J. Pickard and B. D. Simons, Nature Physics **1**, 42 (2005).
- [35] X. Blase, A. Rubio, S. G. Louie and M. L. Cohen, Phys. Rev. B **51**, 6868 (1995).
- [36] A. Koma, K. Miki, H. Suematsu, T. Ohno and H.

- Kamimura, Phys. Rev. B **34**, 2434 (1986).
- [37] H. Schulz and K. H. Thiemann, Acta Cryst. **A35**, 309 (1979).
- [38] R. Buczko, G. Duscher, S. J. Pennycook and S. T. Pantelides, Phys. Rev. Lett. **85**, 2168 (2000).
- [39] A. Soininen, Academic Dissertation, University of Helsinki (2001).
- [40] E. L. Shirley, Phys. Rev. Lett. **80**, 794 (1998); Eric L. Shirley, J. A. Soininen, G. P. Zhang, J. A. Carlisle, T. A. Callcott, D. L. Ederer, L. J. Terminello and R. C. C. Perera, J. of Electron Spectrosc. Relat. Phenom. **114-116**, 939 (2001).
- [41] J. C. Boettger, Phys. Rev. B **33**, 6788 (1986).
- [42] A. R. Oganov, M. J. Gillan, G. D. Price, J. Chem. Phys. **118**, 10174 (2003).
- [43] J. L. Feldman, B. M. Klein, M. J. Mehl and H. Krakauer, Phys. Rev. B **42**, 2752 (1990).
- [44] D. A. Young, A. K. McMahan and M. Ross, Phys. Rev. B **24**, 5119 (1981).
- [45] S. Fahy, K. J. Chang, S. G. Louie and M. L. Cohen, Phys. Rev. B **35**, 5856 (1987).
- [46] R.M. Wentzcovitch, K. J. Chang and M. L. Cohen, Phys. Rev. B **34**, 1071 (1986).
- [47] D. L. Camphausen, G. A. N. Connell and W. Paul, Phys. Rev. Lett. **26**, 184 (1971).
- [48] K. Kim, W. R. L. Lambrecht and B. Segall, Phys. Rev. B **53**, 16310 (1996).
- [49] A. K. McMahan, Physica B+C, **139-140**, 31 (1986); A. K. McMahan and R. C. Albers, Phys. Rev. Lett. **49**, 1198 (1982).
- [50] S. Ves, U. Schwarz, N. E. Christensen, K. Syassen and M. Cardona, Phys. Rev. B **42**, 9113 (1990).
- [51] P. E. Van Camp, V. E. Van Doren and J. T. Devreese, Phys. Rev. B **38**, 9906 (1988).
- [52] J. Cl erouin, Y. Laudernet, V. Recoules and S. Mazevet, Phys. Rev. B **72**, 155122 (2005).
- [53] A. Zunger and A. J. Freeman, Phys. Rev. B **16**, 2901 (1977).